

CORNER STRENGTH OF INVESTMENT CASTING SHELLS

W. Everhart, S. Lekakh and V. Richards

Department of Materials Science and Engineering, Missouri University of Science and Technology, Rolla, MO, USA

J. Chen, H. Li and K. Chandrashekhara

Department of Mechanical and Aerospace Engineering, Missouri University of Science and Technology, Rolla, MO, USA

Copyright © 2013 American Foundry Society

Abstract

During the investment casting process, the shell is subjected to high internal pressure and thermal stress, particularly during pattern removal and when pouring steel into the free standing ceramic shell. Most testing methods investigate the properties of the ceramic shell in flat regions while cracks typically form in the sharp corners and edge regions. The corners and edge regions have different structure and thickness when compared to flat regions and experience large mechanical stress during processing. In this study, experimental methods were combined with finite element modeling to predict failure stress in the internal corner regions of the shell. The model takes into

consideration the mechanical properties of the ceramic shell to determine the stress developed during loading. The effect of shell porosity on stress concentration in sharp corners was evaluated. A general equation was developed to predict the force necessary for crack formation in the shell based on various geometric variables. The results from the model were experimentally verified and the failure stress in flat and corner regions of the shell were compared in order to develop an improved equation.

Keywords: investment casting, ceramic shell, stress, crack

Introduction

The investment casting process is generally used to produce small, thin walled castings with high detail. The process starts with the manufacture of a pattern. The most common material for patterns is wax but different types of polymeric foam and laser stereolithography patterns are also used.^{1,2} The pattern is dipped in slurry made of ceramic binder and flour usually containing some combination of fused silica, zircon, alumina, or other ceramic material. Refractory granules referred to as stucco are then applied to the wet slurry coating. The combination of slurry and stucco makes a single coat which is allowed to dry before the next coat is applied. The shell building process generally consists of one or two prime coats, designed to provide a better surface finish for the casting, four to ten back up coats, designed to add strength to the shell, and a seal coat, designed to seal the stucco of the final backup coat.^{3,4} The structure in corners of the shell can be different from flat regions due to the placement of the stucco. Variation of the structure can cause these regions of the shell to break under smaller loads.⁵ The pattern is then removed from the shell by melting or decomposition in an autoclave or furnace. Whether done as a part of pattern removal, or as an additional firing process, the ceramic is sintered to increase the strength of the shell enough to withstand the pressure of liquid metal. Liquid metal is then poured into the free standing shell, which is usually preheated.

Many new pattern materials, such as polymeric foams, have greater coefficients of thermal expansion than wax which can increase the chance of shell cracking during pattern removal.⁶ Due to the majority of these cracks forming along the edges and in the corners of the shell, the properties of these areas are of interest. Investment casting shells often have a complex geometry with sharp internal corners and edges which also initiate stress concentration in changes in pore structure. Work has been done to determine the strength of these areas of the investment shell compared to flat regions.⁷ A test method has been developed using a wedge design. Along with this test method, an equation to determine the failure stress (σ , MPa) in the corner region of the wedge was developed:

$$\sigma = \frac{12.2(\sin \theta \cos \theta Fd)}{WT^2} \quad \text{Eqn. 1}$$

where: θ is the angle (from vertical) of the splitter used during the wedge test, d is length, W is width, and T is the thickness of the sample in mm and F is the failure force in N. Equation 1 follows from a simplified stress analysis and does not consider the angle of the sample or the radius of the corner of the sample. It is well known that the radius of the corner is important due to its effect as a stress concentrator.⁸

Investment casting shells have large porosity due to the stuccoing process. Recently published experimental strength and porosity data of various porous ceramics were reviewed

and these data were compared with those calculated from both the minimum contact solid area (MCA) and the pore stress concentration effect (SCE) models.⁹ According to the MCA model, the mechanical strength of fully dense ceramic decreases exponentially with increasing volume fraction porosity (P):

$$\sigma = \sigma_0 \exp(-bP) \quad \text{Eqn. 2}$$

where: b is an empirical parameter related to the minimum solid area and dependent on the pore structure.

According to the SCE model, the resulting fracture strength-porosity relationship for all ceramic materials can be given by a power equation of the form:

$$\sigma = \sigma_0(1 - P)^\eta \quad \text{Eqn. 3}$$

where: η is related directly to the pore structure (shape and orientation of the pores with respect to the stress axis) and the Poisson's ratio of the material.

It was observed that the MCA model better matched the experimental results of ceramics in the low volume fraction porosity range ($P < 0.25$) range, whereas larger volume fraction porosity ceramics ($P > 0.35$) are more accurately modeled by the SCE model.⁸ Because investment casting shells have between 0.2 and 0.3 volume fraction porosity,^{9,10} both models could be used to predict the flexural breaking stress in flat regions typically obtained from three or four-point bend tests.¹¹ Stress concentration at both the corner radius of the investment shell and its internal pores could interact, affecting the overall stress development in the shell.

The objective of this research was to develop a test procedure to determine the properties of investment casting shells in flat and edge regions and to investigate the effect of shell geometry on the force required to break the shell. Finite element modeling, experimental wedge testing and microstructural analysis were used to determine the effect of shell geometry and structure on crack formation in shell corners.

Experimental Procedures

A triangular prism pattern was designed to compare the shell strength in flat region and along the edge (Fig. 1b). Triangular prism patterns were 152 mm (6'') tall, 76 mm (3'') wide with a 15° angle from vertical (30° included angle) with a variation of 0.5 mm (0.02'') to 5.0 mm (0.2'') corner radius (Fig. 1a). Several wedge and flat specimens for three-point bend test-

ing were made from the shell built around the triangular prism pattern. Flat specimens were also tested with an artificial stress concentrator approximately 1.0 mm (0.04'') depth and 0.5 mm (0.02'') wide (Fig. 1c) that was cut with a diamond blade. Five specimens for each condition were tested.

The slurry was made of colloidal silica binder (Megasol BI) and fused silica flour (-200 mesh). Slurry viscosity was measured by a Brookfield DVII+ Pro Viscometer. All coatings were applied at 800 ± 100 cP viscosity which is equivalent to 19-22 seconds on a #5 Zahn cup. The patterns were submerged in the slurry until completely covered and then removed and suspended over the slurry for approximately 50 seconds allowing for excess slurry to drain. During this time, the pattern was rotated and allowed to drain from different points to promote an even coating. A uniform distribution of stucco was then applied using the rainfall method by continuously rotating the pattern so that all surfaces were directly impacted by the falling stucco until no more stucco would adhere to the surface. The stucco for the prime coat was composed of granular zircon (-100+200 mesh) and the stucco for the back-up coats was fused silica (-30+50 mesh). The seal coat used no stucco. The samples were dried for at least four hours between coats. The shells were fabricated with one prime coat, five backup coats, and one seal coat. After the seal coat was applied, the samples dried for another 24 hours. Acetone was used to remove the expendable polystyrene (EPS) foam patterns without altering the "green" strength (unfired strength) of the shell.

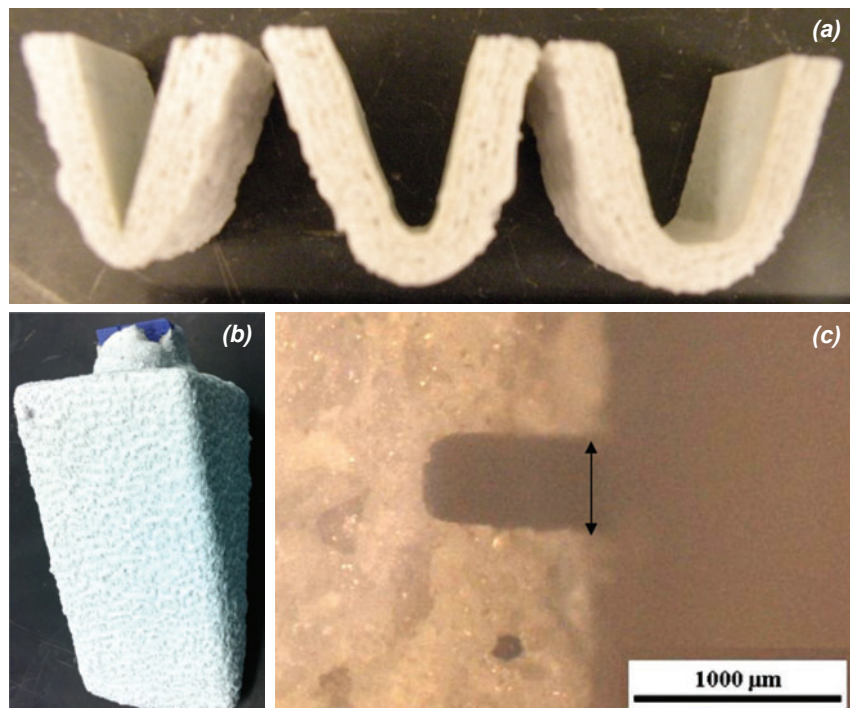


Figure 1. (a) Wedge specimens, (b) shell built around foam pattern and (c) the artificial stress concentrator used in flat specimens.

The mechanical properties of the shell were explored in the green and fired conditions (1000°C for 1 hour) for flat and corner regions with variations in corner geometry. Each wedge was carefully sectioned using a wet diamond saw. Flat 30x75 mm (1.18'' x 2.95'') samples were prepared from the top area of the wedge sides and 50 mm (2'') tall corner samples were taken from the bottom of the wedge. To study the effect of the artificial stress concentrator, 500 μm wide notches were made using a high precision diamond Allied Techcut saw. Assessment of the properties in the green condition is important for stress analysis during pattern removal and the prevention of shell cracking. Properties in the fired condition are important to determine the shell integrity during steel pouring. The maximum stress at rupture and elastic modulus of the flat specimens were determined using three-point bend testing of the shells performed at room temperature according to ASTM C1161.¹² The tip of the testing fixture had a radius of 3.0 mm (2''). The porosity of the shells was measured using two methods; Archimedes method (ASTM C20)¹³ and helium pycnometry.

Modeling Procedures

A static displacement controlled finite element model has been developed in this work to determine the stress in the ceramic shell at the edges where cracks often initiate and propagate. The finite element model is capable of finding the applied force on the wedge and the stress on the ceramic shell. Geometric and contact nonlinearities are incorporated into the model. To save computational cost, one quarter of the wedge and ceramic shell has been modeled and sym-

metric boundary conditions were applied (Figure 2b). The model was cut along the x-z plane and the y-z plane. Shells with different combinations of width (w), length (d), radius (r), and shell angle (α) were modeled. The loading wedge used in the model had an angle θ of 22.5° from vertical (Figure 2a). In addition, the three-bend point test was modeled for specimens with and without an artificial stress concentrator (Figure 2).

ABAQUS¹⁴ version 6.9 was used to conduct all the simulation work. Denser mesh was used in critical regions, such as the internal corner of the ceramic shell and the contact surface between the shell and the wedge (12,600 8-node linear brick elements have been used for the ceramic shell). The wedge is assumed to be a rigid body, and 12,142 4-node 3-D bilinear rigid quadrilateral elements were used. To mesh the wedge test 3D model, all edges were initially seeded by numbers. In order to obtain higher result accuracy and to save computational cost, additional seeds and biased seeds were used in critical regions and fewer seeds were used in regions that were of less interest, and hex mesh shape and structured mesh technique were used. The finite element meshes for the V-shaped ceramic shell with and without a spherical pore are shown in Figure 2b and 2c. The contact properties between the shell and the wedge were defined to allow slip in order to simulate the actual experimental process. Maximum principal stress was identified to monitor the actual stress variations in the shell because the shell is a brittle material with high porosity. The formulation for static displacement controlled mechanical analysis can be written as:

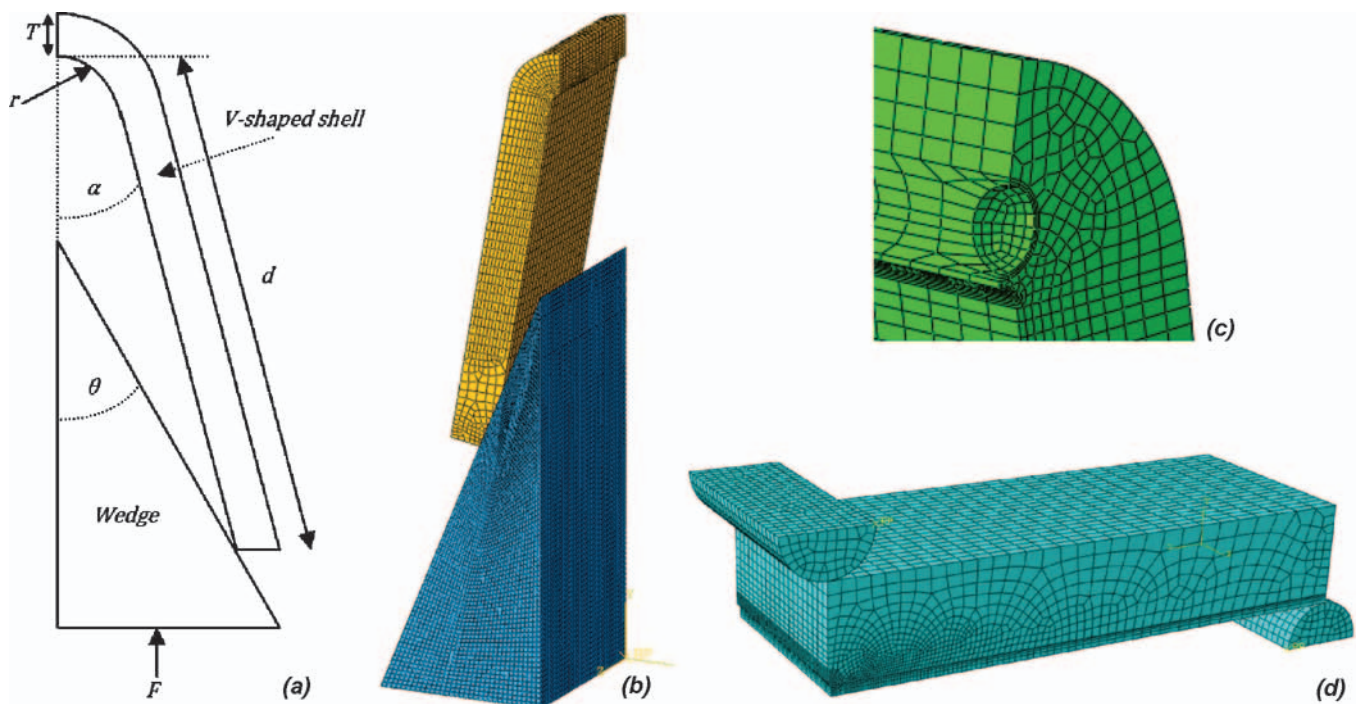


Figure 2. (a) Schematic of the wedge test, (b) mesh of finite element model of wedge specimen without and (c) with pore, (d) mesh of three-point bend test flat specimen with notch.

$$[K^e] \{U^e\} = \{F^e\} \quad \text{Eqn. 4}$$

where: $[K^e] = \int_v [B]^T [C] [B] dv$

$\{U^e\} = \{u, v, w\}^T$

$[K^e]$ is the stiffness matrix, $\{F^e\}$ is mechanical loadings, B is the strain-displacement function, C is the elasticity matrix, and $\{u, v, w\}^T$ are displacement components in a rectangular Cartesian coordinate system.

Modeling Results

To investigate the reduction in breaking stress caused by porosity, the effect of an artificial stress concentrator on stress development in three-point bend tests was modeled. According to the model the artificial stress concentrator (with 250 μm radius) localized stress and caused a significant increase in stress (Fig. 3). The modeled stress concentrator (with 250 μm radius) increased the local stress during the three-point bend test by a factor of four.

To determine possible interactions between internal pores and corner radius during loading in the wedge specimen, a model of the wedge with an individual pore was developed (Fig. 4a). A modeled spherical pore had variations in radius from 0.25 mm (0.01'') to 0.75 mm (0.03''). The pores with these radii were observed in the studied shells. A worst case scenario was modeled when the one large individual spherical pore was located on the corner of the shell. This approximation allowed the team to avoid computational complications with

using multiple randomly located pores. Shell geometry and load were held constant with a variation in corner radius. Decreasing corner radius in the model without a pore exponentially increased stress concentration with an exponential power of -0.27. In the shell with a pore, decreasing the corner radius also increased stress concentration exponentially, but the exponential power was decreased (Fig. 4b). Larger pore size caused a more significant change because the area of stress concentration was larger. It was found that the relationship between corner radius and stress shown by largest pore (0.75 mm (0.03'') radius) was closest to the relationship of experimental samples. The large pore was assumed to have the same effect as multiple smaller pores. The exponential power used to correct for the interaction of pores and the corner radius was -0.16. When the corner radius was larger than the pore size, stress concentration

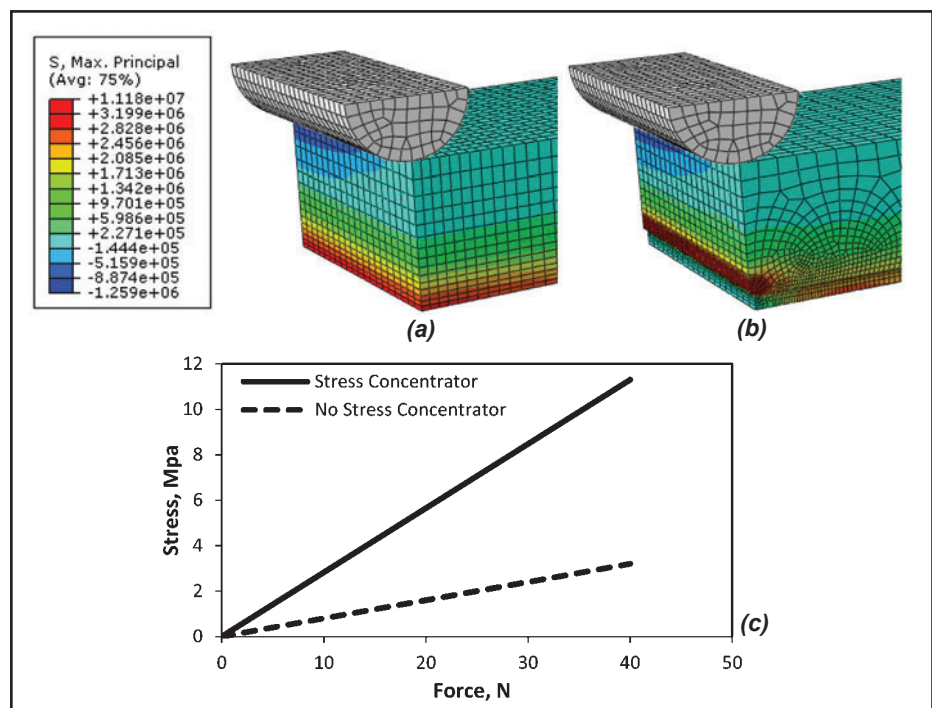


Figure 3. (a) Illustration of calculated stress distribution in three-point bended specimen without and (b) with notch, and (c) stress versus loading force for both cases.

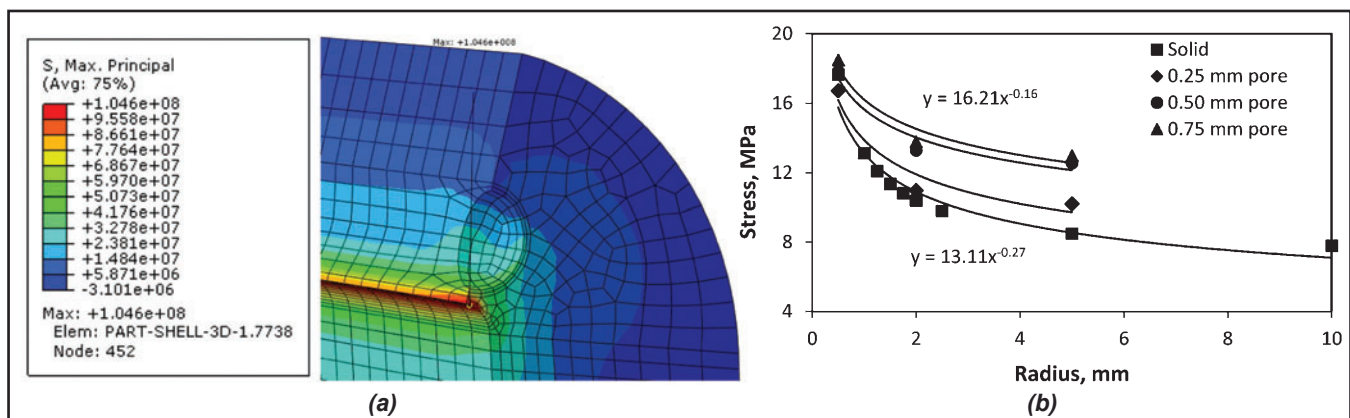


Figure 4. (a) Illustration of calculated stress distribution in loaded wedge with 0.75 mm (0.03'') radius pore and (b) the effect of radius of wedge and pore on stress in shell at constant applied force and dimensions.

was controlled by the porosity. For smaller radius corners the pore had no significant effect.

In addition to corner radius (r), the thickness (t), width (w), loading distance (d), and the angles θ and α were separately varied in the finite element model to determine their effect on the stress in the wedge for a given force. The results were used to formulate Eqn. 5 that fits the modeling results for a fully dense ceramic:

$$\sigma = \frac{16.7Fd \cos(\theta - \alpha)r^{-0.27}}{WT^2} \quad \text{Eqn. 5}$$

Presence of a single pore decreased the effect of radius on stress concentration (Fig. 4b) and Eqn. 5 was modified to account for this difference:

$$\sigma = \frac{20Fd \cos(\theta - \alpha)r^{-0.16}}{WT^2} \quad \text{Eqn. 6}$$

The finite element modeling results for both the dense wedge model and the wedge model with a pore were compared to the values approximated from Eqns. 5 and 6 as well as values obtained using previously published⁷ Eqn. 1. The suggested equations take into consideration all geometric variables and were applicable to a greater range of possible geometries for modeled wedge specimens with and without a pore (Figure 5).

Experimental Results and Discussion

Microstructures of the various corner geometries were prepared to investigate the effect of microstructural features of the shell on its properties. In flat regions of the shell the various layers of shell can be seen and the fine stucco of the prime coat is fairly uniform and thick (Figure 6). Both corner images show similar structure to the flat region except for differences in the prime coat. The structure of a 5 mm (0.2") radius corner is shown in Figure 6b and shows a uniform layer of prime coat stucco that is thinner than observed in the flat sample. The 0.5 mm (0.02") radius corner shows almost no prime coat stucco at the corner (Figure 6c). Elongated porosity with a radius of 0.2-0.7 mm (0.008-0.03") can be observed in the images.

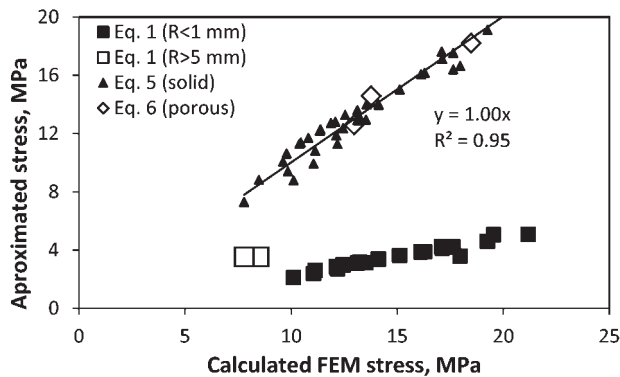


Figure 5. The relationship between the finite element modeling results and stress values calculated by Equations 5 and 6 compared to Equation 1.

To determine the effect of internal porosity on the breaking stress of the shell both the experimental and modeling results of three-point bend testing with a stress concentrator were compared. The flexural failure stress was calculated from experimentally measured breaking force (F) using:

$$\sigma = \frac{3Fl}{2WT^2} \quad \text{Eqn. 7}$$

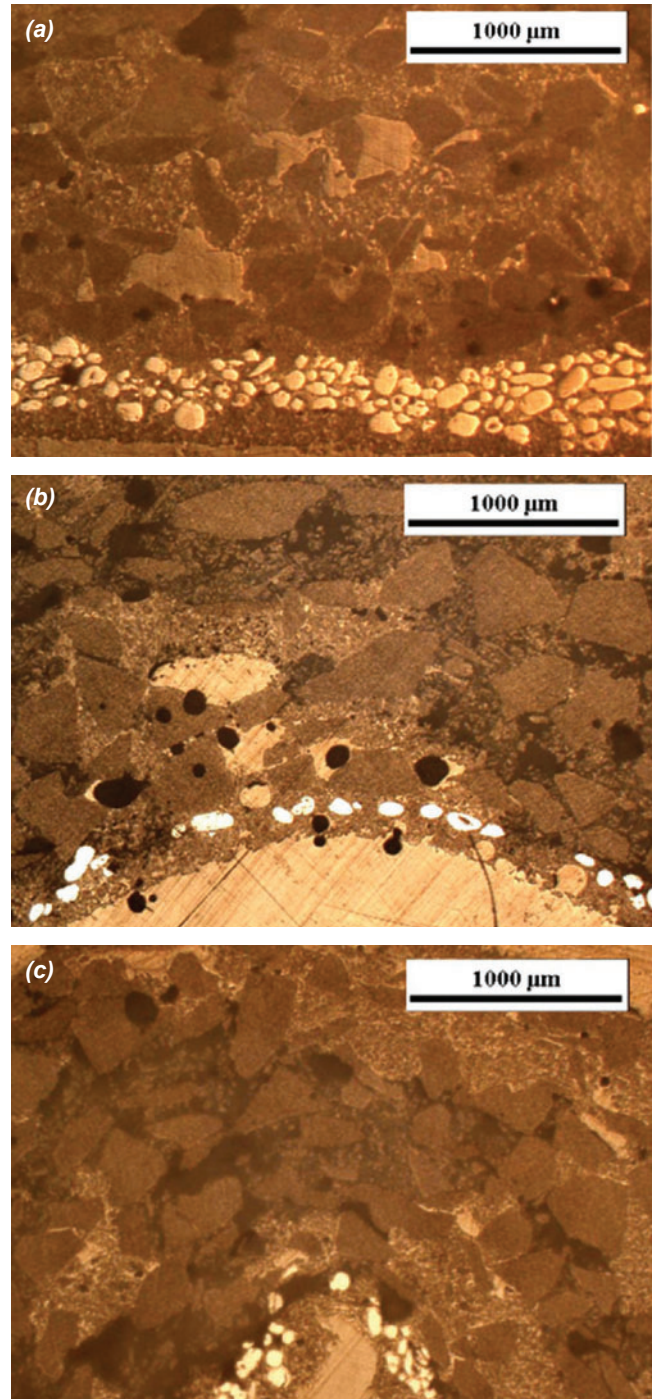


Figure 6. (a) Microstructures of the investment casting shell in flat regions, (b) wedges with 5 mm (0.2") and (c) 0.5 mm (0.02") corner radii that shows differences in the structure of the prime coat stucco.

Where: F is the applied force, l is the span length, W is sample width, and T is the sample thickness. The results from these tests were compared to the finite element modeling results in Table 1. The model showed a large increase in stress in the shell with a notch whereas the experimental results show no significant difference in breaking stress. These results demonstrate that internal porosity is as significant a stress concentrator as the artificially added “notch.”

Tests were performed on green shells and fired shells (1 hour @ 1000°C). The MCA model (Eq. 2) was applied to Eq. 6 to correct for the change in thickness caused by porosity. With this correction applied Eq. 6 becomes:

$$\sigma = k \frac{20Fd \cos(\theta - \alpha)r^{-0.16}}{WT^2} \quad \text{Eqn. 8}$$

Where: k is the correction value for porosity determined from the MCA model. Using the stress values from the three-point bend modeling cases (with and without a stress concentrator) and the volume percent porosity of the shells that were tested (0.3), the empirical parameter b in Eqn. 2 was calculated to be 4.0. Using Eqn. 2 the value of k was calculated to be 0.3. This lowers the failure stress from Eq. 7 to a range that fits with three-point bend test results (Figure 7a). Equation 8 fits experimental data best when the maximum observed pore radius is smaller than the corner radius. When the pore radius is larger than the corner radius the model overestimates the fracture strength. To estimate breaking stress values for corners with a radius smaller than 2.0 mm (0.08”) it is recommended that the value of the corner radius used in Eqn. 8 should be 2.0 mm (0.08”). By substituting a larger corner radius value the resulting stress fits with expected values. When there is a high volume fraction of po-

rosity near the inside corner of the shell, caused by either a higher number of pores or larger pores, the amount of stress concentration increases. Variation in the sample wedge angle causes a slight difference in strain rate in the fracture zone, this change in strain rate showed no significant effect on the breaking stress in the model or experimental results. Equation 8 was applied to both fired and unfired samples and the properties in flat and wedge regions were comparable for both cases (Figure 7b).

Conclusions

The strength of corner and edge regions was analyzed. Shell porosity was found to significantly reduce the effect of corner radius on the amount of stress concentration. Experimental methods were combined with finite element modeling to develop the following equation to predict stress in corner regions of the shell:

$$\sigma = k \frac{20Fd \cos(\theta - \alpha)r^{-0.16}}{WT^2} \quad \text{Eqn. 8}$$

Equation 8 predicted stress accurately for corner radii 2.0 mm (0.08”) or larger. The results from the model were experimentally verified after using the MCA model (Eq. 2) to adjust stress values for the effect of porosity. The failure stress of flat and corner regions of the shell were found to be similar for both fired and un-fired shells.

Acknowledgements

The authors would like to thank U.S. Army Armament Research, Development & Engineering Center (ARDEC) - Benét Labs for funding this research under contract num-

Table 1. Summary of Modeling and Experimental Results for Flat Three-Point Bend Test of Flat Specimen

Case	Length, mm	Width, mm	Thickness, mm	Notch	Experimental flexural failure stress, MPa	FEM calculated flexural failure stress, MPa
1	76.2	29.0	7.1	Yes	3.7	11.3
2				No	3.7	3.2

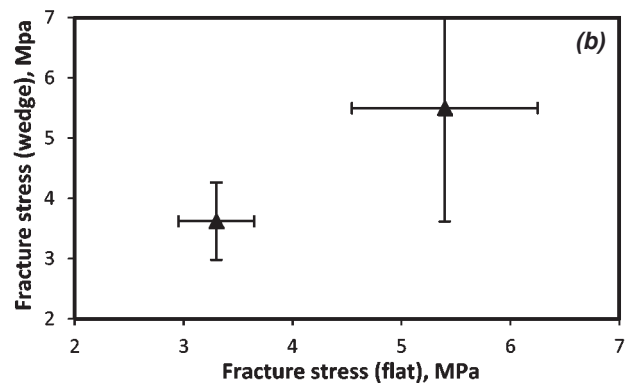
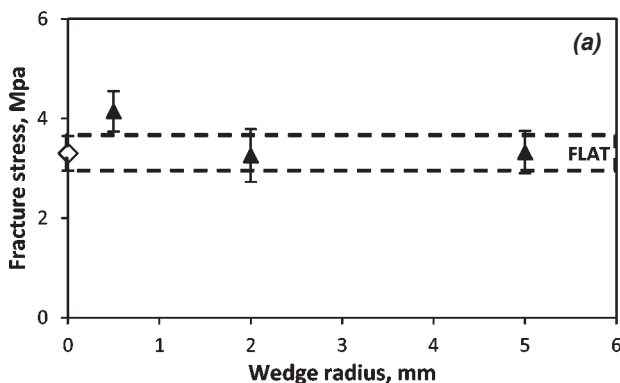


Figure 7. (a) Comparison of fracture stress of “green” flat and wedge specimens with different radii and (b) comparison of fracture stresses for fired and unfired samples.

ber W15QKN-07-2-0004. The authors wish to recognize the assistance of Tom Towey, Katherine Ramsey and Jamie Fitzgerald for sample preparation. The results and opinions contained in this paper are those of the authors and not necessarily those of U.S. Army Benet Laboratories.

REFERENCES

1. Foster, G., "Flashfire Dewax for Today's Investment Casting Foundry," Investment Casting Institute 42nd Annual Meeting, pp. 2:1-2:11, Atlanta, Georgia; USA; 25-28 (September 1994).
2. Yao, W. L.; Leu, Ming C., "Analysis of Shell Cracking in Investment Casting with Laser Stereolithography Patterns," *Rapid Prototyping Journal*, vol. 5, no. 1 (March 1999).
3. Capadona, J.A., "Slurry Process Control in Production can "Crack Down" on Shell Cracking," *Incast*, vol. 4, no. 4, pp. 10-12 (April 1991).
4. Guerra, M., Schiefelbein, G.W., "Review of Shell Components, Shell Characteristics and Properties: Refractory Selection for Primary Shell Coat," Investment Casting Institute 42nd Annual Meeting, Atlanta, Georgia; USA; 25-28 September 1994.
5. Kline, D., Controlling Strength and Permeability of Silica Investment Casting Molds, Missouri University of Science and Technology, Thesis, pp. 46-47 (2010).
6. Kline, D., Lekakh, S., Mahimkar, C., Richards, V., "Crack Formation in Ceramic Shell During Foam Pattern Firing," Technical and Operating Conference, Chicago, Illinois; USA (December 2009).
7. Hyde, R., Leyland, S., Withey, P., Jones, S., "Evaluation of the Mechanical Properties of Investment Casting Shells," 22nd Investment Casting Conference (1995).
8. Peterson, R. E., "*Peterson's Stress Concentration Factors*," John Wiley and Sons Inc., pp.18-20 (1961).
9. Kruse, B. L., Richards, V. L., "Thermal and Moisture Characterization during Autoclave Dewaxing in Investment Casting," Proceedings of the 59th SFSA T&O Conference, No. 5.5 (2005).
10. Mahimkar, C., Thermo-physical Properties Measurement and Steel-Ceramic Shell Interactions in Investment Casting, Missouri University of Science and Technology, Thesis, pp. 76 (2011).
11. Nyongesa, F. W., Aduda, B.O., "Fracture Strength of Porous Ceramics: Stress Concentration vs Minimum Solid Area Models," *African Journal of Science and Technology*, Science and Engineering Series, vol. 5, no. 2, pp. 19-27 (Dec.2004).
12. ASTM C1161, "Standard Test Method for Flexural Strength of Advanced Ceramics at Ambient Temperature," ASTM International, www.astm.org (2002).
13. ASTM C20, "Standard Test Methods for Apparent Porosity, Water Absorption, Apparent Specific Gravity, and Bulk Density of Burned Refractory Brick and Shapes by Boiling Water," ASTM International, www.astm.org (2000).
14. ABAQUS Version 6.9. Manual, Dassault Systèmes S.A., Software Applications for FEA & CAE (2009).

Technical Review and Discussion

Corner Strength of Investment Casting Shells

W. Everhart, S. Lekakh, V. Richards, J. Chen, H. Li and K. Chandrashekhara; Missouri University of Science and Technology, Rolla, MO, USA

Reviewers: Whether the FEA model is based on continuum materials assumption or porous materials assumption was not answered clearly. The findings of this paper mechanically make sense. Porous materials' break stress is insensitive to local stress concentrators. However, the continuum FEA modeling method used to simulate intrinsic porous shell materials is still questionable in my opinion. Especially this assumption "The large pore was assumed to have the same effect as multiple smaller pores." This statement is in conflict to well-known experiment results.

Authors: It is correct that the FEA model is based on continuum material assumption. To analyze the effects of internal (porosity) and external (radius of wedge) stress concentrators and their interaction, the FEA local/global approach was used and the results were compared to ex-

perimental data. In particular, in the local approach, stress in the wedge with different corner radii having a single different diameter spherical pore was calculated. The material around pore was modeled as a continuous media, however, this local approach allowed us to evaluate interaction of internal and external stress concentrators. The pore was located near the internal corner and we assumed that it was the scenario worth considering when compared to other pore locations. This assumption allowed us to avoid multiple calculations for randomly located pores. We tested the real wedge shells with evaluation of near corner porosity and also tested flat sample with and without artificial stress concentrator (notch). After that, FEA modeling of breaking force during wedge compression test were done based on continuum material assumption (global approach) where the shell material properties included the effect of internal stress concentrator (porosity). We agree with reviewer that statement in article "The large pore was assumed to have the same effect as multiple smaller pores" was not investigated. Further research will be conducted to develop finite element models based on "more real" porous structure assumption, for example when the porous shell has larger and dispersed pores at the internal corner of wedge.